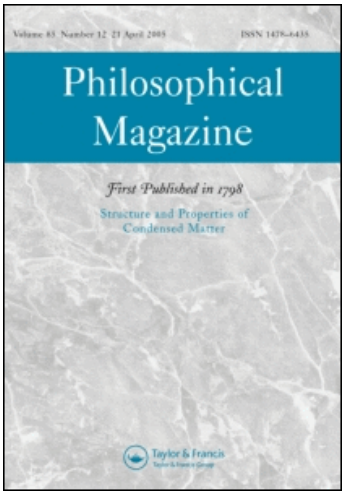

Philosophical Magazine
Publication details, including instructions for authors and subscription information:
http://www.informaworld.com/smpp/title~content=t713695589

Defects in CaF_2 caused by long-time irradiation and their response to annealing

Vojtěch Vlček[ab]; Jakub Čížek[c]; Jan Drahokoupil[de]; Jan Valenta[f]; Nobuyoshi Miyajima[b]; Roman Skála[ag]
[a] Faculty of Sciences, Charles University in Prague, Prague 2, Czech Republic [b] Bayerisches Geoinstitut, Universität Bayreuth, Bayreuth, Germany [c] Faculty of Mathematics and Physics, Charles University in Prague, Praha 8, Czech Republic [d] Institute of Physics of the ASCR, Prague 8, Czech Republic [e] Faculty of Nuclear Sciences and Physical Engineering, Czech Technical University, Prague 2, Czech Republic [f] Faculty of Mathematics and Physics, Charles University in Prague, Praha 2, Czech Republic [g] Institute of Geology of the ASCR, Prague 6, Czech Republic

Online publication date: 28 May 2010

To cite this Article Vlček, Vojtěch , Čížek, Jakub , Drahokoupil, Jan , Valenta, Jan , Miyajima, Nobuyoshi and Skála, Roman(2010) 'Defects in CaF_2 caused by long-time irradiation and their response to annealing', Philosophical Magazine, 90: 20, 2749 — 2769
To link to this Article: DOI: 10.1080/14786431003745385
URL: http://dx.doi.org/10.1080/14786431003745385

Philosophical Magazine
Vol. 90, No. 20, 14 July 2010, 2749–2769

Taylor & Francis
Taylor & Francis Group

Defects in CaF_2 caused by long-time irradiation and their response to annealing

Vojtěch Vlček[ab]*, Jakub Čížek[c], Jan Drahokoupil[de], Jan Valenta[f], Nobuyoshi Miyajima[b] and Roman Skála[ag]

[a]*Faculty of Sciences, Charles University in Prague, Albertov 6, CZ – 12000, Prague 2, Czech Republic;* [b]*Bayerisches Geoinstitut, Universität Bayreuth, D-95440, Bayreuth, Germany;* [c]*Faculty of Mathematics and Physics, Charles University in Prague, V Holešovičkách 2, CZ-18000, Praha 8, Czech Republic;* [d]*Institute of Physics of the ASCR, v. v. i., Na Slovance 2, CZ-182 21, Prague 8, Czech Republic;* [e]*Faculty of Nuclear Sciences and Physical Engineering, Czech Technical University, Trojanova 13, CZ-120 00, Prague 2, Czech Republic;* [f]*Faculty of Mathematics and Physics, Charles University in Prague, Ke Karlovu 3, CZ-12000, Praha 2, Czech Republic;* [g]*Institute of Geology of the ASCR, v. v. i., Rozvojová 269, CZ-16500, Prague 6, Czech Republic*

(*Received 28 October 2009; final version received 17 February 2010*)

Samples of CaF_2 irradiated for millions of years in nature were studied by several methods, including X-Ray diffraction, positron annihilation spectroscopy (PAS), photoluminescence spectroscopy (PLS) and transmission electron microscopy (TEM). It was found that the unexpectedly high density of radiation-induced defects present in the fluorite structure (documented by TEM) causes significant micro-strains. Even annealing up to 450°C cannot completely remove these micro-strains, which are stabilised by impurities. PAS and subsequent theoretical calculations revealed the behaviour of the defects during heating. The PL spectra of irradiated fluorite were also interpreted.

Keywords: fluorite; microstructure; defect; positron annihilation spectroscopy; photoluminescence spectroscopy; transmission electron microscopy; X-ray diffraction

1. Introduction

Radiation-induced defects in the fluorite (CaF_2) structure have been investigated only in artificially irradiated samples in recent studies (e.g. [1–4]). However, the response of the structure to long-term irradiation (of the order of a million years) is essential for understanding the processes of formation and the stability of defect centres. These recent studies showed that the radiation damage in fluorite should reach a saturation level and then there should be a dynamic balance of creation and annihilation of the centres, resulting in minimum strains within the lattice. Understanding how the fluorite structure responds to a long-term irradiation is important for its potential use under conditions of prolonged exposure to radiation

*Corresponding author. Email: vojtech.vlcek@uni-bayreuth.de

ISSN 1478–6435 print/ISSN 1478–6443 online

DOI: 10.1080/14786431003745385
http://www.informaworld.com

in applications such as containment of radioactive waste (as proposed in [2]), special optics or applications in electrotechnics (e.g. [5]). As a consequence, we chose natural samples of fluorite to evaluate effect of the long-term irradiation on CaF_2 structure. A microstructure analysis from X-ray powder diffraction data, positron annihilation spectroscopy (PAS), photoluminescence spectroscopy (PLS) and transmission electron microscopy (TEM) was used to decipher the behaviour of fluorite under prolonged radiation.

2. Experimental methods and sample description

2.1. *Samples*

A natural CaF_2 sample from Kletno (Poland) has been exposed to radiation emitted by surrounding uraninite (UO_2) for millions of years. It has a dark purple colour and dim surface. This sample was assumed to display the highest degree of irradiation damage. Fluorite from Vlastějovice (Czech Republic) has been irradiated by allanite (Ce-silicate). The activity of this mineral is several times lower in comparison to uraninite. Hence, the sample from Vlastějovice was assumed to represent a low-irradiated CaF_2. A non-irradiated fluorite sample from the locality Jílové u Děčína (Czech Republic) and a synthetic standard (Suprapur, Merck) were used as reference materials.

2.2. *X-ray diffraction*

X-ray powder diffraction patterns were collected with a PANalytical X'Pert Pro diffractometer equipped with an X'Celerator position-sensitive detector and a secondary graphite monochromator (Institute of Physics, Academy of Sciences of the Czech Republic). Data were step-scanned over the range from 10° to 150° 2Θ with 0.05° step size and 300 s counting time per step. The cobalt tube was operated at a 40 kV voltage and 30 mA current.

The naturally irradiated fluorite sample from Kletno annealed up to 450°C was subsequently X-ray irradiated on conventional X-ray source MIKROMETA (Faculty of Science, Charles University in Prague) with unfiltered radiation from Cu tube operated at 40 kV and 30 mA.

The diffraction peak parameters were fitted using Rietveld refinement procedure with Le-Bail fit as implemented in the HighScore software (PANalytical). A Williamson–Hall plot (described in [6]) was used to visualise the difference between crystallite size and a micro-strain peak broadening.

2.3. *PAS*

A $^{22}Na_2CO_3$ positron source with activity of 1.5 MBq deposited on a 2 μm thick mylar foil was used in PAS measurements. The source was placed in the centre of a small cylindrical chamber with a diameter of 10 mm and height of 5 mm. Subsequently, the chamber was completely filled with the sample powder and closed. Dimensions of the chamber ensured that virtually all positrons were stopped inside the chamber and, thereby, annihilated in the studied powder.

Positron-lifetime measurements were performed using a digital spectrometer described in [7,8]. The spectrometer was equipped with BaF_2 scintillators and fast photomultipliers (Hamamatsu H3378). Detector pulses are directly digitised using a couple of 8-bit ultra-fast digitisers Acqiris DC 211 with sampling frequency of 4 GHz. Analysis of digitised pulses and construction of positron-lifetime spectrum was performed off-line using the so-called integral true constant fraction technique described in [9]. The spectrometer exhibits excellent time resolution of 145 ps (full width at half-maximum (FWHM) ^{22}Na). At least 10^7 positron annihilation events were accumulated in each positron lifetime spectrum. Decomposition of positron-lifetime spectra into exponential components was performed using a maximum likelihood procedure described in [10]. The source contribution to positron-lifetime spectra consisted of two weak components with lifetimes of ~368 ps and ~1.5 ns and corresponding intensities of ~8% and ~1%. These components represent a contribution of positrons annihilated directly in Na_2CO_3 source and the covering mylar foils.

Coincidence Doppler broadening (CDB) studies were carried out using a spectrometer [11] equipped with two high-purity Ge detectors. The overall energy resolution of the CDB spectrometer was (1.02 ± 0.01) keV at 511 keV. At least 10^8 annihilation events were collected in each of two-dimensional γ-ray energy spectra, which were subsequently reduced into two one-dimensional cuts representing the resolution function of spectrometer and Doppler broadened annihilation profile. In this paper CDB results are presented as ratio curves with respect to a well annealed bulk Mg (99.99%) reference specimen.

Theoretical calculations of positron parameters were performed from first principles using an approach based on density functional theory. The positron wave function was calculated within the so-called conventional scheme employing the atomic superposition (ATSUP) method [12]. The electron–positron correlation was treated within the local density approximation (LDA) using the scheme developed by Boronski and Nieminen [13] with the correction [14] for incomplete positron screening with high-frequency dielectric constants, $\varepsilon_\infty = 6.8$ [15]. A cubic structure with lattice parameter $a = 5.46305$ Å [16] was adopted for CaF_2. A supercell approach was used for calculations of positron parameters for CaF_2 crystal containing defects. The calculations were performed on 768 atom-based supercells. Vacancies or vacancy agglomerates were created simply by removing the appropriate number of atoms from the supercell.

The high momentum part (HMP) of the momentum distribution of electrons that annihilated positrons was performed using ATSUP-based approach according to the scheme described in [17,18]. The electron–positron correlation was treated using the LDA approach [13,14] and also by the generalised gradient approximation (GGA) scheme developed by Barbiellini et al. [19,20]. Only the contribution from positrons annihilated by localised core electrons were considered in the calculations. Hence, comparison of calculated HMP curves with experiment is meaningful only in the high momentum range, $p > (10 \times 10^{-3}) m_0 c$, where contribution of positrons annihilated by core electrons dominates. The following orbitals were considered as core electrons and included in the calculations of HMP curves: Ca $1s^2$, $2s^2$, $2p^6$, $3s^2$, $3p^6$; F $1s^2$, $2s^2$, $2p^5$; Mg $1s^2$, $2s^2$, $2p^6$.

The final one-dimensional HMP curve, which can be compared to the experimental CDB spectrum, was obtained by summing up the contributions of the core states of all atoms in the system and integrating over the high-momentum tail. In order to compare the calculated HMP curves to experimental CDB spectra, they have to be properly normalised. The areas of the experimental CDB spectra were scaled to unity, whereas the areas below the theoretical HMP curves were set equal to λ_{core}/λ, where λ_{core} is the annihilation rate with all core electrons of the system and λ is the total annihilation rate, i.e. the inverse of positron lifetime. In order to mimic the effect of the finite resolution of the experimental setup, the theoretical HMP curves were convoluted with a Gaussian with FWHM of $(4.0 \times 10^{-3})\, m_0 c$.

2.4. *PLS*

Both high- and low-irradiated fluorite and the reference sample of synthetic CaF_2 were investigated by photoluminescence micro-spectroscopy. In addition, the high-irradiated sample annealed to 450°C was investigated after exposure to X-rays. The PL emission was collected by the inverted microscope Olympus IX-71 with 20× magnification objective lens and detected with the liquid-nitrogen cooled BI-CCD camera attached to the imaging spectrometer Acton SpectraPro 2150i. The data were measured at room temperature. PL was excited by a diode laser emitting at 405 nm. Several measurements were made on different positions of each sample in order to obtain reasonable statistics. The data were fitted by Fityk software [21] using split Gaussian function, which refines peak half-widths separately.

2.5. *TEM*

Powdered fluorite samples (from Kletno, Vlastějovice and synthetic CaF_2) were placed onto TEM copper grids coated with carbon holey films. The microscope used to study the samples was a Philips CM 20 FEG (at the Bayerisches Geoinstitut, Universität Bayreuth, Germany) operated at 200 kV voltage. The samples were imaged under bright field, dark field and weak-beam dark field conditions. High-resolution TEM images were also acquired. Selected area electron diffraction was used to define the orientation of the samples. In order to investigate the existence of some impurities, energy-dispersive X-ray spectra were also collected with 60 s live time.

3. Results and discussion

3.1. *X-ray diffraction*

The diffraction peaks of the irradiated sample are broadened mainly due to micro-strain that is caused by defects and lattice deformations; the domain size broadening has negligible contribution. The diffraction patterns were collected during *in situ* heating at different temperatures to obtain information about the structure recovery caused by annealing. Subsequent peak-broadening analysis using the Williamson–Hall method [6] confirmed the expected decrease of

micro-strain values. The data plotted in the Williamson–Hall graph (Figure 1) shows that the main recovery process is started at temperatures higher than 300°C. To determine possible slow kinetics at lower temperatures, several measurements were done at 300°C (total heating lasted 8 h); however, no change of micro-strain was observed.

The annealed sample (up to 450°C) became colourless after the experiment, yet some micro-strains remained. We assume that some defects persist and are not affected by heating. It should be noted that the reference samples from Jílové and the synthetic CaF_2 also showed non-zero values of micro-strain. Nevertheless, these micro-strain values were substantially lower than those observed in the annealed and X-ray irradiated samples.

Another interesting feature noted in the annealed samples was a colour change from colourless to purple upon irradiation by the X-ray beam during the XRD study. The stability of colouration depended on the time of X-ray irradiation. After a short irradiation (about 1 h) the colour dissipates in about three days; however, after irradiation that lasted more than 500 h the colour was stable. X-ray irradiation did not affect the microstructure characteristics of the sample (no peak-broadening was observable in the diffraction pattern). This confirms the different character of the colour centres and the defects causing microdeformation.

3.2. *PAS*

3.2.1. *Theoretical calculations*

First principles calculations of positron characteristics were performed in order to identify defects in CaF_2 samples. Table 1 shows calculated positron lifetimes for various positron states in CaF_2 crystal. The calculated positron density in the (110)

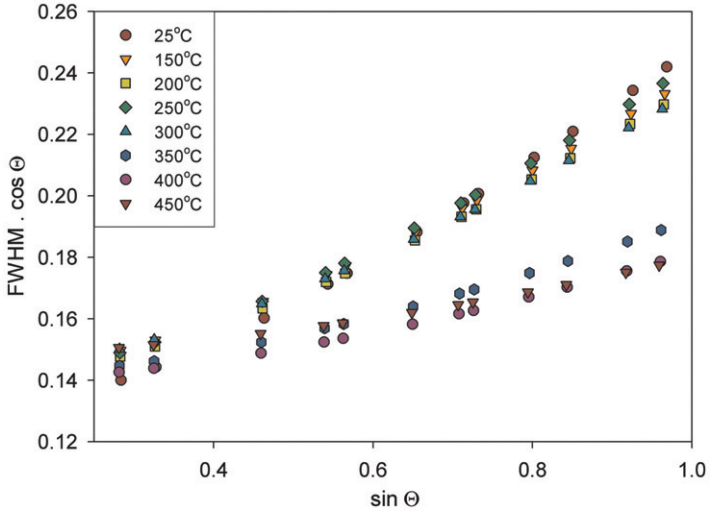

Figure 1. (Colour online). Williamson–Hall plot showing the data obtained through whole powder pattern fitting. The source powder patterns were measured *in situ* during annealing. The micro-strain is proportional to the slope of the linear regression.

Table 1. Results of the first principles calculations of positron parameters (positron lifetime, τ, and positron binding energy to defect, E_B) for various positron states in CaF_2.

	τ (ps)	E_B (eV)
Bulk	171.5	–
F-vacancy	172.1	0.008
Ca-vacancy	225.9	1.680

plane for a perfect defect-free CaF_2 crystal is plotted in Figure 2a. Positrons in a perfect CaF_2 crystal are delocalised in the lattice in the form of modulated Bloch-like waves. The calculated bulk positron lifetime in a perfect CaF_2 crystal is 171.5 ps.

Figure 2b shows the calculated positron density in CaF_2 containing an F-vacancy. Although there is a slight enhancement of positron density in the vicinity of the F-vacancy, there is still a significant probability of finding positrons elsewhere. Hence, the F-vacancy is too shallow a trap and incapable of confining a positron. This is confirmed by the positron lifetime, which approaches the bulk positron lifetime in CaF_2 and also by a negligible positron binding energy to the F-vacancy (see Table 1).

On the other hand, the Ca-vacancy is a deep positron trap. Figure 2c shows that positron is completely localised in a Ca-vacancy. The calculated lifetime of a positron trapped in a Ca-vacancy is 225.9 ps and the positron binding energy to this defect is 1.68 eV.

Thus, theoretical calculations clearly demonstrated that F-vacancies are very shallow traps that are "invisible" to positrons. On the other hand, Ca-vacancies are strong traps that can undoubtedly be detected by PAS.

It is known that F-vacancies produced in CaF_2 by irradiation aggregate and form fluorine voids [22–25]. This process leads to formation of metallic Ca inclusions in CaF_2 where fluorine voids occur and only Ca atoms remain in their sites. For this reason, it is important to examine the possibility of positron trapping in aggregates of F-vacancies. Figure 3 shows the results of first principles calculations of positron parameters for F-vacancy aggregates of various sizes. As can be seen in Figure 3, both positron lifetime and positron binding energy to an aggregate of F-vacancies increases with increasing number of F-vacancies (i.e. increasing size of fluorine void). The calculated positron density for a CaF_2 crystal containing an F-divacancy is plotted in Figure 4a. Similar to the F-vacancy, the F-divacancy is also too shallow a trap to confine a positron. This is demonstrated not only by the absence of positron localisation, but also by the calculated positron lifetime, which is close the bulk positron lifetime in perfect CaF_2, and the very small positron binding energy to F-divacancy.

A remarkable increase of positron binding energy occurs for a F-tetravacancy (see Figure 3b). The calculated positron density for a CaF_2 crystal containing an F-tetravacancy, plotted in Figure 4b, shows a significant increase of positron localisation. Hence, the F-tetravacancy becomes capable of positron trapping and can be detected by PAS. Even larger aggregates of F-vacancies are yet deeper traps

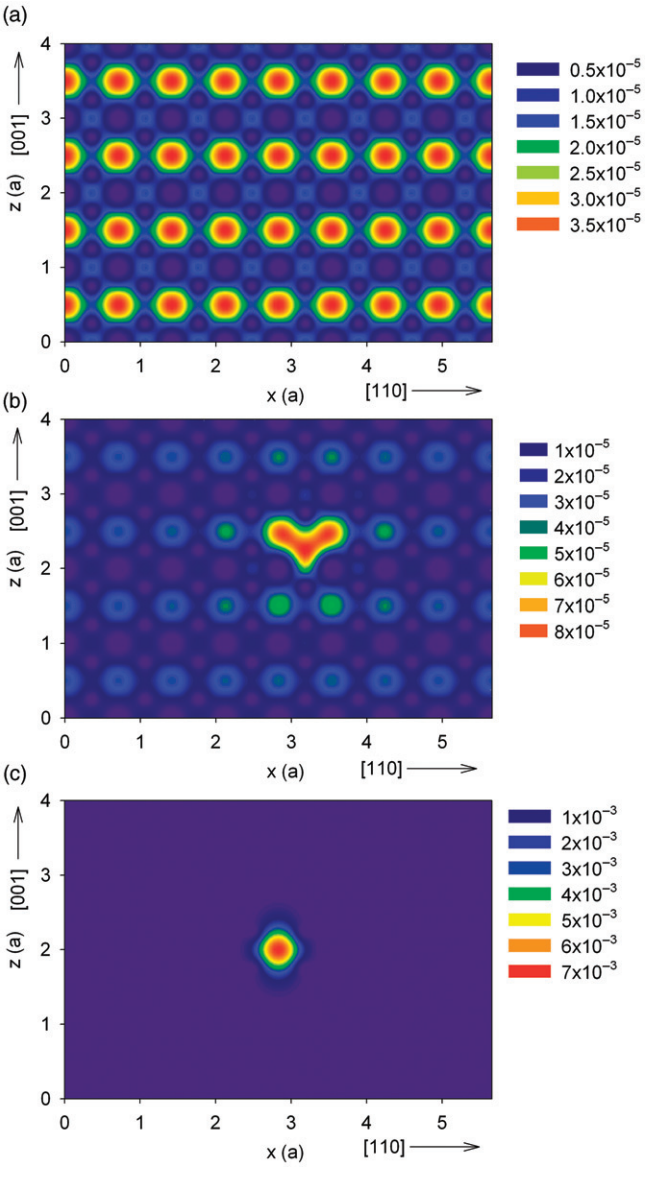

Figure 2. (Colour online). Calculated positron density in (110) plane for (a) a perfect CaF_2 crystal, (b) CaF_2 crystal containing F-vacancy, and (c) CaF_2 crystal containing Ca-vacancy. Positron density is expressed in atomic units; distances are shown in units of CaF_2 lattice parameter.

characterised by a longer positron lifetime and higher positron binding energy (Figure 3). Figure 5a shows the calculated positron density for an agglomerate of 8 F-vacancies. It can be seen that the positron is fully localised and that the lifetime of positrons trapped at this defect is comparable to that of a positron trapped in a Ca-vacancy (Figure 3a).

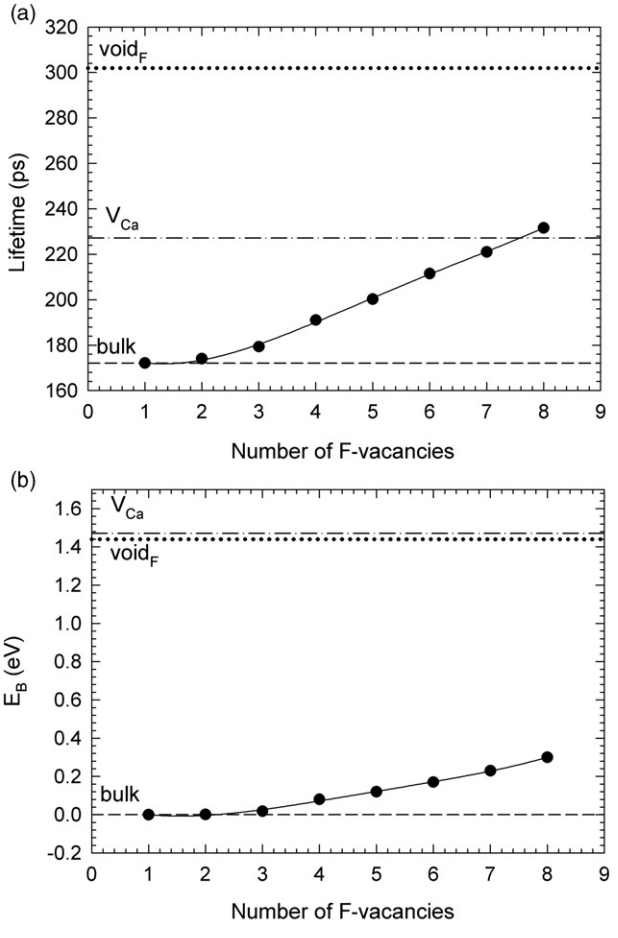

Figure 3. Results of first principle calculations of positron parameters for F-vacancy agglomerates: (a) positron lifetime and (b) positron binding energy as a function of number of F-vacancies in the agglomerate. Dashed lines show positron parameters for a perfect CaF_2 crystal, dash-doted lines show positron parameters for Ca-vacancy and dotted lines show positron parameters for a large fluorine void.

Calculated positron characteristics for a CaF_2 supercell with all F atoms removed represents an extreme case and simulates a very large fluorine void; it is plotted in Figure 5b. The figure illustrates that the positron is delocalised inside the fluorine void and is located mostly in the empty sites in fluorine sub-lattice. The lifetime of a positron delocalised in a very large fluorine void is 301.9 ps and the positron binding energy is 1.44 eV.

3.2.2. *Positron lifetime spectroscopy*

The reference non-irradiated CaF_2 powder exhibits a two-component positron lifetime spectrum (Table 2). The shorter component with lifetime $\tau_1 = (110 \pm 10)$ ps

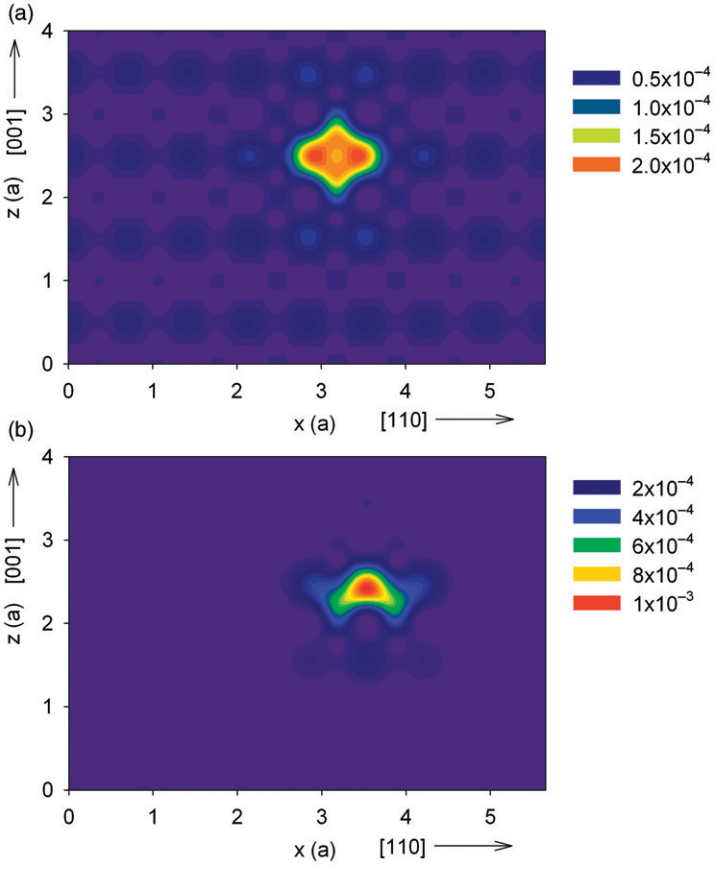

Figure 4. (Colour online). Calculated positron density in (110) plane for a CaF_2 crystal containing (a) F-divacancy, (b) F-tetravacancy. Positron density is expressed in atomic units; distances are shown in units of CaF_2 lattice parameter.

and relative intensity $I_1 = (41 \pm 1)\%$ can be attributed to free, delocalised positrons. The longer component with lifetime $\tau_2 = (322 \pm 2)$ ps and relative intensity $I_2 = (59 \pm 1)\%$ is a contribution of positrons trapped at defects. The lifetime τ_2 of this component is longer then lifetimes calculated for aggregates of F-vacancies (Figure 3a). It is even longer than the upper limit for F-vacancy aggregates, i.e. positron lifetime of 302 ps calculated for a large fluorine void. Hence, the longer component in positron lifetime spectrum of reference CaF_2 powder represents a contribution of positrons trapped at larger defects (voids) containing not only F-vacancies, but also Ca-vacancies.

In the frame of the two-state simple trapping model [26] the quantity

$$\tau_f = \left(\frac{I_1}{\tau_1} + \frac{I_2}{\tau_2}\right)^{-1} \quad (1)$$

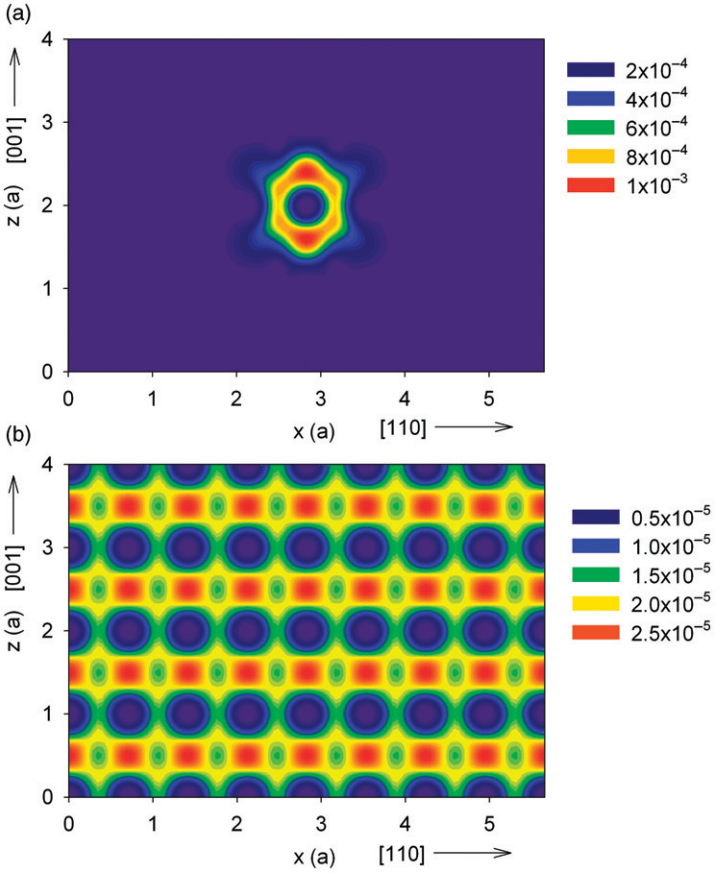

Figure 5. (Colour online). Calculated positron density in (110) plane for a CaF_2 crystal containing: (a) an agglomerate of 8 F-vacancies; (b) a large fluorine void. Positron density is expressed in atomic units; distances are shown in units of CaF_2 lattice parameter.

Table 2. Results of positron lifetime measurements of CaF_2 powders.

Sample	τ_1 (ps)	I_1 (%)	τ_2 (ps)	I_2 (%)
Reference, non-irradiated	110 ± 10	41 ± 1	322 ± 2	59 ± 1
Irradiated, Kletno	197 ± 1	67 ± 1	335 ± 4	33 ± 1

equals to the bulk positron lifetime

$$\tau_f \equiv \tau_B. \tag{2}$$

Equations (1)–(2) are frequently used to check the consistency of spectrum decomposition with the two-state simple trapping model. For the reference CaF_2 powder we obtained $\tau_f = (179 \pm 8)$ ps, which is in a good agreement with the calculated bulk positron lifetime in a perfect CaF_2 crystal shown in Table 1.

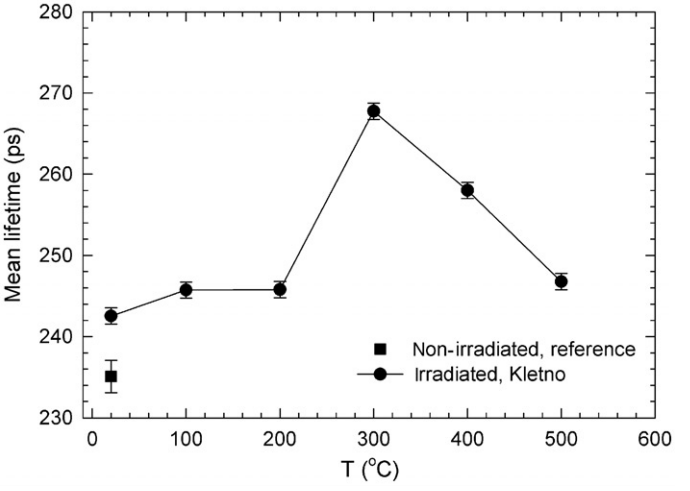

Figure 6. Temperature dependence of the mean positron lifetime, τ_{mean}, for naturally irradiated CaF_2 powder from Kletno.

This confirms that assumptions of two-state simple trapping model (i.e. a single type of uniformly distributed defects) are fulfilled in the case of virgin CaF_2 powder. Note that positron annihilations studies of CaF_2 crystals were performed by angular-correlation [27] but no positron lifetime investigations of CaF_2 crystals have been performed so far to the best of our knowledge.

The irradiated natural CaF_2 powder from Kletno exhibits a two-component positron lifetime spectrum. Lifetimes, τ_1 and τ_2, of these components are longer than the bulk positron lifetime in CaF_2. Thus, both these components represent a contribution of positrons trapped at defects. The longer component exhibits lifetime $\tau_2 = (335 \pm 4)$ ps, which is comparable with the lifetime τ_2 measured on the reference powder. Hence, similar to the reference powder, the longer component in the irradiated CaF_2 can be attributed to positrons trapped at larger voids containing both F-vacancies and Ca-vacancies. On the other hand, the shorter component with lifetime $\tau_1 = (197 \pm 1)$ ps represents a contribution of positrons trapped at new defects created by irradiation. It is well known that agglomerates of F-vacancies are formed in irradiated CaF_2 [22–25]. Indeed, the lifetime τ_1 corresponds to the calculated lifetime of positrons trapped at an agglomerate of 4 F-vacancies (Figure 3a).

The irradiated CaF_2 powder from Kletno was subsequently subjected to isochronal annealing. The mean positron lifetime

$$\tau_{mean} = \sum_i I_i \tau_i, \tag{3}$$

the centre of mass of the positron-lifetime spectrum, is a robust single parameter, which is not influenced by mutual correlations of fitted parameters. Figure 6 shows the dependence of the mean positron lifetime on the annealing temperature for irradiated CaF_2 powder from Kletno. There was a strong increase of τ_{mean} in the

temperature range from 200 to 300°C, indicating a change of defect structure. Finally, above 300°C, the mean lifetime decreases.

More information can be obtained from decomposition of positron lifetime spectra. At all annealing temperatures positron-lifetime spectra of irradiated CaF_2 are well fitted by two components. Lifetimes of these two components are plotted in Figure 7a as a function of annealing temperature, whereas Figure 7b shows the temperature dependence of the intensity I_2 of the longer component.

The lifetime τ_1 of positrons trapped at F-vacancy agglomerates gradually increases with annealing temperature (see inset in Figure 7a) indicating the increasing size of the agglomerates. The intensity I_1 of positrons trapped at F-vacancy agglomerates, plotted in Figure 7b, increases remarkably after annealing above

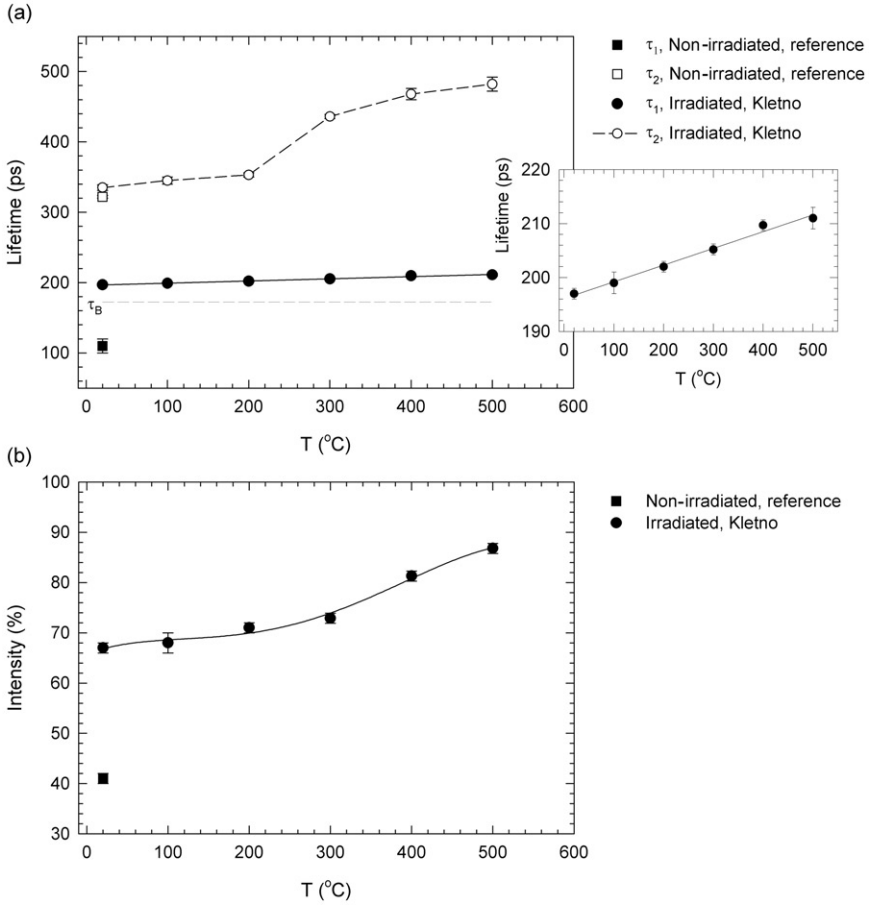

Figure 7. Temperature dependence of (a) lifetimes τ_1, τ_2 of exponential components resolved in positron-lifetime spectrum, (b) the relative intensity I_1 of the shorter component. Results measured on naturally irradiated CaF_2 powder from Kletno are plotted by circles, whereas squares show results for the reference non-irradiated CaF_2 powder. Position of the bulk CaF_2 lifetime is indicated by the dashed line in the upper panel. The inset presents zoomed temperature dependence of the lifetime τ_1.

300°C. This behaviour indicates that agglomeration of irradiation-induced single F-vacancies or very small F-vacancy clusters occurs at temperatures $T \geq 300$°C. Theoretical calculations in Section 3.2.1 demonstrated that isolated F-vacancies or very small F-vacancy agglomerates containing less than 4 F-vacancies cannot be detected by PAS. However, larger agglomerates containing at least 4 F-vacancies are capable of positron trapping and can be detected by PAS. Hence, agglomeration of isolated F-vacancies or very small F-vacancy clusters into larger agglomerates, which takes place at temperatures $T \geq 300$°C, enhances positron trapping to these defects, which is reflected by an increase of intensity I_1. This is accompanied by a gradual increase of lifetime τ_1 of this component due to increasing average size of F-vacancy agglomerates. The lifetime τ_2 of the longer component increases after annealing at 300°C. This could be due to F interstitials (*H*-centres) which become mobile at 300°C and form fluorine bubble-like defects (e.g. as described in [22]) in the sample. Positrons trapped at these fluorine bubbles contribute to the longer component and causes an increase of lifetime τ_2.

3.2.3. *Coincidence Doppler broadening*

Figure 8 shows calculated HMP profiles for a perfect CaF_2 crystal and reference defect-free pure Mg. The experimental curves for a reference non-irradiated CaF_2 powder and a well-annealed bulk Mg are plotted in the figure as well. It is clear that the curves calculated using GGA scheme are in better agreement with experiment than curves calculated using LDA approach. This is due to a well known fact that LDA overestimates positron annihilations with core electrons [21]. Due to this reason only the curves calculated using the GGA scheme will be considered in the further discussion. As was explained in Section 3.2.1, only localised core electrons

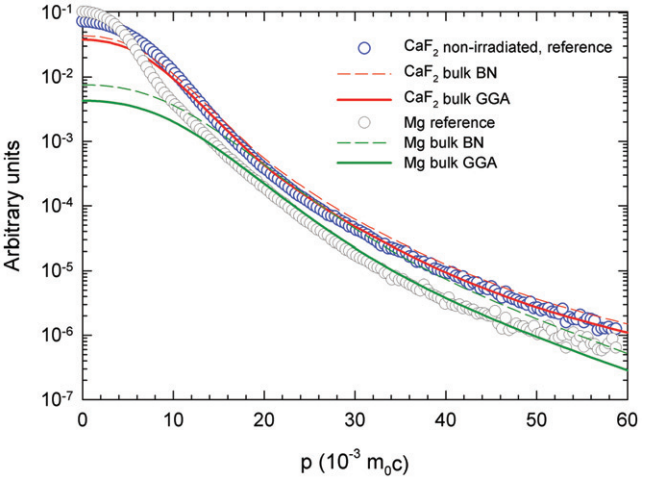

Figure 8. (Colour online). Experimental Doppler broadened annihilation profiles for non-irradiated CaF_2 powder and well-annealed pure Mg reference sample compared with calculated HMP curves for perfect Mg and CaF_2 crystal. Solid and dashed lines show the HMP curves calculated using GGA and LDA approach, respectively.

that retain their atomic character are considered in the calculations of HMP profiles. Low momentum valence electrons were not included in the calculations. Therefore, comparison of calculated curves with experiment is meaningful only in the high momentum range $p > 10 \times 10^{-3}\, m_0 c$, where positron annihilations with localised core electrons dominate. Indeed, as can be seen in Figure 8, experimental curves for reference CaF_2 and Mg are well reproduced by theoretical calculations in the high momentum range $p > 10 \times 10^{-3}\, m_0 c$.

The contributions of various electron orbitals to the calculated HMP profile for a perfect CaF_2 crystal are plotted in Figure 9. From comparison of the experimental profile with theoretical calculations, it is clear that positrons are annihilated mostly by F electrons. This is not surprising because there is an attractive Coulomb interaction between positron and F anions. Thus, in a perfect CaF_2 crystal the overlap of positron density with F anions is significantly larger than with Ca cations (see Figure 2a).

Figure 10 shows the ratio curve (related to Mg reference) for the reference non-irradiated CaF_2 powder and naturally irradiated CaF_2 sample from Kletno in the as-received state and after annealing to various temperatures. The ratio curves exhibit a sharp peak located at $p \sim (9 \times 10^{-3})\, m_0 c$. This is mainly due to contribution of positrons annihilated by fluorine $2p$ electrons. The second important feature is a broad peak at $p \sim (40 \times 10^{-3})\, m_0 c$, which represents a contribution of positrons annihilated by fluorine s-electrons.

The irradiated CaF_2 sample is characterised by a decrease in amplitudes of both peaks in the ratio curves (Figure 10). This confirms that the contribution of positrons annihilated by fluorine electrons is reduced in the irradiated sample. This is in accordance with formation of F-vacancy aggregates detected by positron-lifetime spectroscopy. Contrary to free positrons delocalised in perfect CaF_2 crystal,

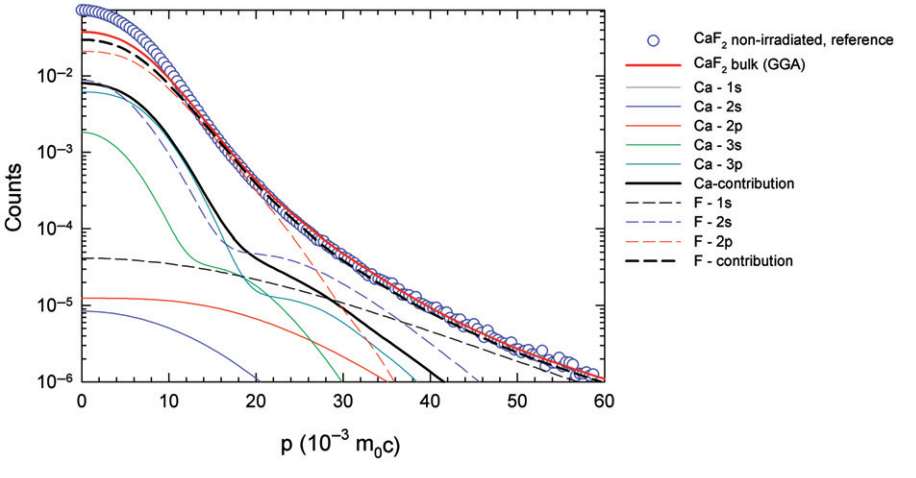

Figure 9. (Colour online). The calculated HMP curve for a perfect CaF_2 crystal with contributions of various core electron orbitals shown. The HMP curve was calculated using the GGA approach. The partial contributions of Ca and F electrons are plotted by solid and dashed lines, respectively. Total contributions of positrons annihilated by Ca and F electrons are also plotted.

positrons localised in F-vacancy aggregates (containing at least 4 F-vacancies) are annihilated mostly by Ca-electrons because fluorine atoms are missing in F-vacancy aggregates. Hence, an increase in positron trapping in F-vacancy aggregates causes a decrease in fraction of positrons annihilated by F-electrons.

This effect can be seen also on the calculated HMP curves plotted in Figure 11. Clearly, the calculated ratio curves for positrons trapped at F-vacancy agglomerates are lower than the curve for a perfect CaF_2 crystal. This is due to reduced contribution of positrons annihilated by F-electrons. The ratio curve for F-vacancy

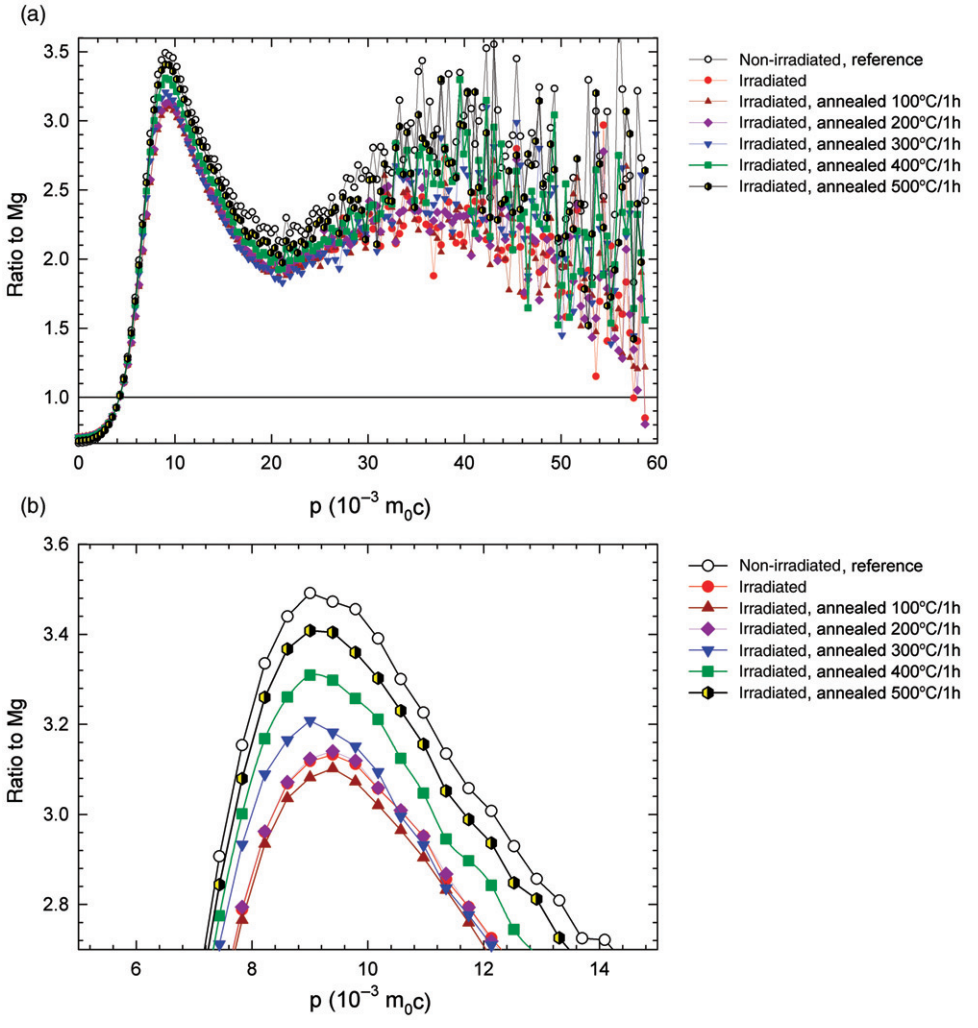

Figure 10. (Colour online). (a) Experimental CDB ratio curves (related to pure Mg reference sample) for virgin, non-irradiated CaF_2 powder and for naturally irradiated CaF_2 from Kletno. The latter sample was measured in the as-received (irradiated) state and after annealing up to various temperatures. (b) A detail of the amplitude of the peak in CDB ratio curves located at momentum $p \approx (9 \times 10^{-3})\ m_0c$.

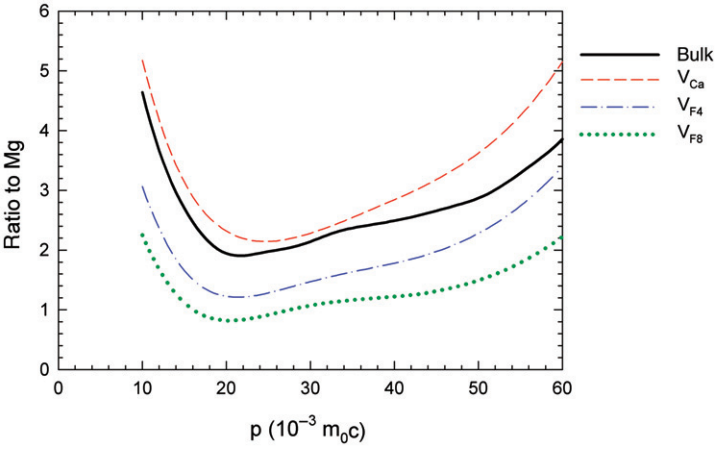

Figure 11. (Colour online). Calculated ratio curves (related to pure Mg) for free positrons annihilating in a perfect CaF_2 crystal (bulk) and positrons trapped at Ca-vacancy (V_{Ca}), agglomerate of 4 F-vacancies (V_{F4}), and agglomerate of 8 F-vacancies (V_{F8}). The ratio curves were calculated using the GGA approach.

agglomerate containing 8 F-vacancies is located below the curve for agglomerate containing 4 vacancies because the contribution of positrons annihilated by F-electrons decreases with increasing size of the agglomerate.

On the other hand, the calculated ratio curve for positrons trapped in a Ca-vacancy is situated above the curve for a perfect CaF_2 because F-atoms occupy the nearest neighbour sites of Ca-vacancy. Hence, there is relatively high probability that it will be annihilated by F-electron, whereas the probability to be annihilated by Ca-electron is negligible.

With increasing temperature the fraction of positrons annihilated by F-electrons firstly decreases due to increasing size of F-vacancy agglomerates (Figure 10b). The lowest contribution of the positrons annihilated by F-electrons was found after annealing at 100°C. Annealing to temperatures above 200°C leads to an increase of the fraction of positrons annihilated by F-electrons because positrons become trapped at fluorine bubbles, i.e. the fraction of positrons annihilated by F-electrons increases. This enhancement of the fraction of positrons annihilated by F-electrons agrees with the increase of lifetime τ_2 observed by positron-lifetime spectroscopy (Figure 7a) and explained by formation of fluorine bubbles.

3.3. *PLS*

The detected PL spectra revealed the distinct behaviour of irradiated and non-irradiated fluorites. Six different emission bands with peaks at about 431, 479, 514, 587, 644, and 720 nm were observed. They are labelled E_1 to E_6, respectively, and are listed in Table 3. However, the natural reference fluorite sample from Jílové exhibits no emission bands, thus confirming the absence of impurities or luminescent defects. The E_2 and E_5 bands are present in the synthetic reference sample and some

Table 3. Observed emission bands and their assignment.

Emission	λ (nm)	Assignment
E_1	431	*F*-centres bound to substituent
E_2	479	Non-radiation-induced defects
E_3	514	*F*-centres bound to substituent
E_4	587	*F*-/*H*-centres
E_5	644	Non-radiation-induced defects
E_6	720	Electron-defect bound state

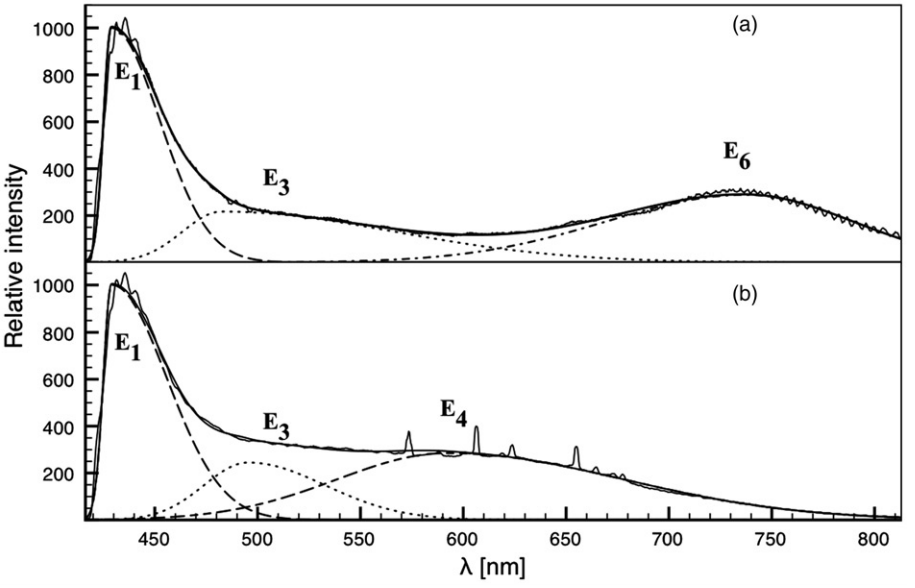

Figure 12. Photoluminescence spectra of long-time irradiated CaF_2 untreated (a) and after annealing up to 450°C (b).

irradiated samples and seem to be unaffected by heating or X-ray irradiation. Therefore these bands cannot be related to radiation-induced defects. We assigned the E_2 emission peak (corresponding to 2.59 eV) to oxygen centres (e.g. as in [28]).

For the irradiated samples the E_1, E_3 and E_6 emission bands are characteristic (Figure 12). The first one has the highest intensity and low FWHM (i.e. narrow energy distribution). It corresponds to energy of 2.88 eV and it is not affected by annealing or further X-ray irradiation. The E_3 is a broad emission peak corresponding to energy of 2.41 eV and its position is not affected by annealing. The E_6 has a broad FWHM and its centre corresponds to an energy of 1.72 eV. This emission is not present in the annealed samples, which became colourless upon annealing, but the E_6 emission reappears again in samples irradiated by X-rays after being annealed.

The E_1 emission band can be assigned either to *F*-centres or their clusters or to the impurities, which cause emissions slightly shifted to lower wavelengths. This effect was discussed in previous studies for, e.g. Zn^+ [4] or Eu^{2+} [29]. Since impurities are common in all natural samples both impurities and *F*-centres can be expected to contribute to the E_1 emission band. Defect centres in natural samples could be bound to the foreign atoms in the structure. This binding makes the defects more stable and resistant to heating. However, the exact character of the substituents is difficult to identify as even very low concentrations (ppm) can cause the luminescent effect and an additional study would be necessary to obtain the desired information. As the E_3 emission has behaviour similar to E_1 it probably represents the same type of luminescence centres. The interpretation of the E_6 emission band seems to be more complicated as it is influenced by heating and X-ray irradiation; it will be discussed later.

In the annealed samples the additional E_4 emission appears; corresponds to energy of 2.11 eV. However, it is placed in the region of a broad absorption band of *F*- or *H*-centres (see [4]). We suppose that the E_4 emission is present in irradiated sample before heating but it is absorbed within the sample. The small emission bands of different peak shape and very low FWHM visible on Figure 12b are most likely emissions of impurities. As they should not be affected by heating, their presence only in the spectrum of annealed CaF_2 indicates that the (*F*- and *H*-centres) absorption band disappeared.

Annealed samples of fluorite when X-ray irradiated exhibited the same PL spectra as untreated samples. As the XRD results showed that no new structural defects are formed (described in Section 3.1) we assume that the E_6 emission is connected with some centres, which cannot be detected by XRD. The *F*-centres, which are known to be present in the irradiated CaF_2 samples, are considered as most probable candidates. Hence, one should take into account thermal stability of *F*-centres. Most probably electron is released from *F*-centre during heating and the following X-ray irradiation causes the electron trapping again. It is in agreement with the observation that the reference non-irradiated material, which does not contain *F*-centres, does not change its colour in X-ray beam. These processes (electron releasing and trapping) can also explain the E_6 emission band and its disappearance due to annealing.

3.4. *TEM*

Samples of high- and low-irradiated fluorite and the reference sample of synthetic CaF_2 were investigated by TEM. The TEM-EDS analysis showed no mutual inter-sample chemical differences within the instrument limits. An increasing defect concentration depending on radiation source activity was observed. The reference material showed no defects observable by TEM. However, in the low irradiated samples from Vlastějovice dislocation loops are documented (Figure 13a). This is in good agreement with the results of previous studies [3]. The Kletno sample contains an unexpectedly high density of defects, as illustrated in the weak-beam dark-field image shown in Figure 13b. The dislocation density is so high in this case that it makes it almost impossible to distinguish individual dislocations or dislocation loops.

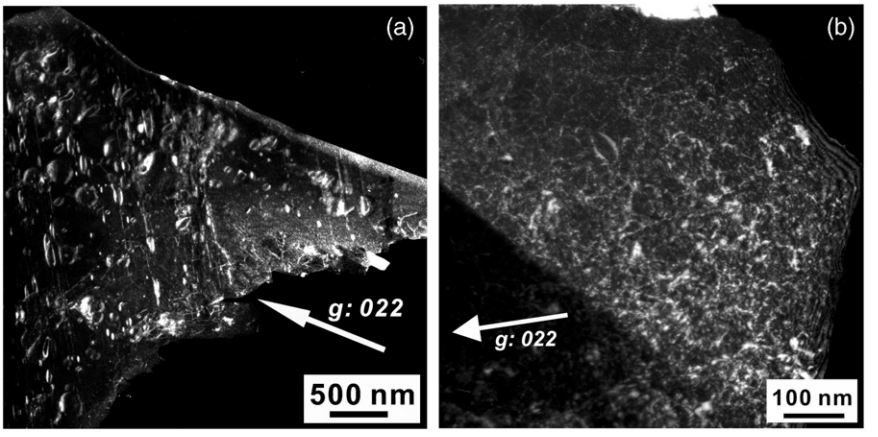

Figure 13. Weak-beam dark-field TEM images with $\mathbf{g} = 022$ of low-irradiated sample from Vlastějovice showing dislocation loops (a) and high-irradiated sample from Kletno displays extreme dislocation density (b).

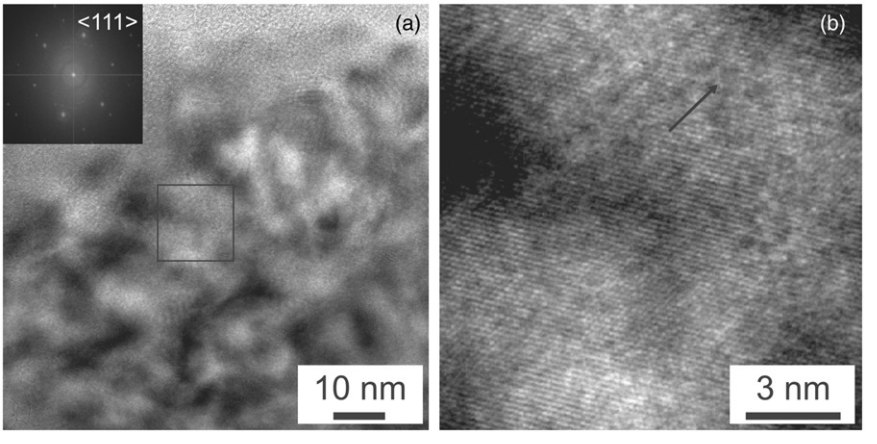

Figure 14. HRTEM images of high-irradiated sample from Kletno (a) and detail of clustered *F*-centres, indicated by the arrow (b). Inset in the left image is a fast Fourier transform image from the squared area, which corresponds to the right image.

The high-resolution TEM image (Figure 14) also confirms the presence of Ca inclusions, previously reported for irradiated samples (e.g. in [30]). The inclusions are produced by *F*-centres clustering and they represent a stable void superlattice. However, the Ca inclusions are not present in the low-irradiated sample. This is probably due to different activities of radiation source.

4. Conclusions

The present study characterises the CaF_2 structure with a high density of radiation-induced defects created by long-term irradiation (of the order of millions

of years) that causes significant lattice micro-strains, whereas some previous studies (e.g. [2]) expected only low lattice strains and consequently also suggested CaF_2 as a candidate for the containment of radioactive waste. These micro-strains decrease rapidly during heating to temperatures exceeding 300°C. However, domain-size broadening was not observed. It was also shown that even after annealing some defects remain present in the structure (documented by non-zero strain observed by XRD or by PL spectra). The first principles PAS calculations showed that agglomerates of F-vacancies are detectable by PAS if they contain at least 4 F-vacancies. The lifetime of positrons trapped at F-vacancy agglomerates depends on size of the agglomerate and falls in the range from 190 to 302 ps. The presented positron lifetime spectroscopic study has not been performed previously and substantially helps to reveal the character of the defects and their behaviour. The detailed measurements showed the presence of *F*-centre agglomerates and their clustering during heating as well as *H*-centre clustering creating free fluorine bubbles in the structure. The knowledge of these processes on the atomistic scale could be necessary for using CaF_2 as a material for high-resolution electron beam lithography or as an insulating layer for semiconductor technology, as discussed in [5].

The defect-related emissions in PL spectra of irradiated CaF_2 were discussed in previous studies (e.g. [4]) without concrete assignment. As the results obtained from other methods revealed the true character of the defects we were able to make this assignment. The PL spectra also showed that the resistant defects are most probably stabilised by impurities; this kind of defects could then significantly influence the quality of optical devices mainly by causing decrease in transmittance. Saturated positron trapping confirmed a high-density of defects in irradiated CaF_2, which was also documented by TEM observations.

Acknowledgements

This work was funded by the The Ministry of Education of The Czech Republic (projects MSM0021620855 and MS0021620834). Authors would like to acknowledge the help of Dr. Viktor Goliáš and Dr. Marek Chvátal. One of the authors (JV) acknowledges the support through the Centre of Nanotechnology and Materials for Nanoelectronics, LC510 (funded by the MSMT CR). RS thanks for the support through the research plan AV0Z30130516 of the Institute of Geology AS CR.

References

[1] M. Boccanfuso, A. Benyagoub, M. Toulemonde, C. Trautmann, K. Schwartz and C. Dufour, Nucl. Instrum. Meth. Phys. Res. B 175–177 (2001) p.590.
[2] L.T. Chadderton, Radiat. Meas. 36 (2003) p.13.
[3] M. Watanabe, T. Noma, K. Yasuda, K. Yasunaga, S. Matsumura and C. Kinoshita, paper presented at the 16th International Microscopy Congress, 2006.
[4] X. Xiang, X.T. Zu, S. Zhu, T.H. Ding and L.M. Wang, Opt. Mater. 28 (2006) p.930.
[5] T. Kogure, K. Saiki, M. Konno and T. Kamino, Mater. Res. Soc. Symp. Proc. 504 (1998) p.183.
[6] H.P. Klug and L.E. Alexander, *X-Ray Diffraction Procedures*, 2nd ed., Wiley, New York, 1974.

[7] F. Bečvář, J. Čížek, I. Procházka and J. Janotová, Nucl. Instrum. Meth. A 539 (2005) p.372.
[8] F. Bečvář, J. Čížek and I. Procházka, Appl. Surf. Sci. 255 (2008) p.111.
[9] F. Bečvář, Nucl. Instrum. Meth. B 261 (2007) p.871.
[10] I. Procházka, I. Novotný and F. Bečvář, Mater. Sci. Forum 255–257 (1997) p.772.
[11] J. Čížek, I. Procházka, B. Smola, I. Stulíková, R. Kužel, Z. Matěj and V. Cherkaska, Phys. Status Solidi (a) 203 (2006) p.466.
[12] M.J. Puska and R.M. Nieminen, J. Phys. F Met. Phys. 13 (1983) p.333.
[13] E. Boroński and R.M. Nieminen, Phys. Rev. B 34 (1986) p.3820.
[14] M.J. Puska, S. Mäkinen, M. Manninen and R.M. Nieminen, Phys. Rev. B 39 (1989) p.7666.
[15] S.K. Dickinson, *Infrared Laser Windows Materials Property Data for ZnSe, KCl, NaCl, CaF_2, SrF_2, BaF_2*, Air Force Cambridge Res. Lab. Report AFCRL-TR-75-0318, 1975.
[16] R.W.G. Wyckoff, *Crystal Structures*, 9th ed., Vol. 1, Interscience/John Wiley, New York, 1963.
[17] M. Alatalo, B. Barbiellini, M. Hakala, H. Kauppinen, T. Korhonen, M.J. Puska, K. Saarinen, P. Hautojärvi and R.M. Nieminen, Phys. Rev. B 54 (1996) p.2397.
[18] J. Kuriplach, A.L. Morales, C. Dauwe, D. Segers and M. Šob, Phys. Rev. B 58 (1998) p.10475.
[19] B. Barbiellini, M.J. Puska, T. Torsti and R.M. Nieminen, Phys. Rev. B 51 (1995) p.7341.
[20] B. Barbiellini, M.J. Puska, T. Korhonen, A. Harju, T. Torsti and R.M. Nieminen, Phys. Rev. B 53 (1996) p.16201.
[21] M. Wojdyr, *Fityk (A curve fitting and data analysis program)*; software available at http://www.unipress.waw.pl/fityk/.
[22] E. Johnson and L.T. Chadderton, Micron 2 (1980) p.247.
[23] E. Johnson and L.T. Chadderton, Radiat. Eff. 79 (1983) p.183.
[24] R. Bebbewitz and D. Smith, Phys. Rev. B 59 (1999) p.8237.
[25] L.P. Cramer, S.C. Langford and J.T. Dickinson, J. Appl. Phys. 99 (2006) p.054305.
[26] R. West, in *Positrons in Solids*, P. Hautojärvi, ed., Springer-Verlag, Berlin, 1979, p.89.
[27] W. Brandt, G. Coussot and R. Paulin, Phys. Rev. Lett. 23 (1969) p.522.
[28] E. Radzhabov, J. Phys.: Condens. Matter 6 (1994) p.9807.
[29] Z. Hao, J. Cai and L. Yi, J. Lumin. 40–41 (1988) p.393.
[30] L.T. Chadderton, E. Johnson and T. Wohlenberg, Phys. Scripta 13 (1976) p.127.